

# Ca<sub>2</sub>Y<sub>2</sub>Cu<sub>5</sub>O<sub>10</sub>: the first frustrated quasi-1D ferromagnet close to criticality

R.O. Kuzian,<sup>1,2</sup> S. Nishimoto,<sup>2</sup> S.-L. Drechsler,<sup>2,\*</sup> J. Málek,<sup>2,3</sup> S. Johnston,<sup>2</sup> J. van den Brink,<sup>2</sup> M. Schmitt,<sup>4</sup> H. Rosner,<sup>4</sup> M. Matsuda,<sup>5</sup> K. Oka,<sup>6</sup> H. Yamaguchi,<sup>6</sup> and T. Ito<sup>7</sup>

<sup>1</sup>*Institute for Problems of Materials Science NASU, Krzhizhanovskogo 3, 03180 Kiev, Ukraine*

<sup>2</sup>*Leibniz-Institut für Festkörper- und Werkstofforschung IFW Dresden, P.O. Box 270116, D-01171 Dresden, Germany*

<sup>3</sup>*Institute of Physics, ASCR, Prague, Czech Republic*

<sup>4</sup>*Max-Planck-Institute for Chemical Physics of Solids, 01187 Dresden, Germany*

<sup>5</sup>*Quantum Condensed Matter Division, Oak Ridge National Laboratory, Oak Ridge, TN 37831, USA*

<sup>6</sup>*AIST, Tsukuba, Ibaraki 305-8562, Japan*

<sup>7</sup>*National Institute of Advanced Industrial Science and Technology (AIST), Tsukuba, Ibaraki 305-8562, Japan*

(Dated: September 22, 2018)

Ca<sub>2</sub>Y<sub>2</sub>Cu<sub>5</sub>O<sub>10</sub> is built up from edge-shared CuO<sub>4</sub> plaquettes forming spin chains. From inelastic neutron scattering data we extract an in-chain nearest neighbor exchange  $J_1 \approx -170$  K and the frustrating next neighbor  $J_2 \approx 32$  K interactions, both significantly larger than previous estimates. The ratio  $\alpha = |J_2/J_1| \approx 0.19$  places the system very close to the critical point  $\alpha_c = 0.25$  of the  $J_1$ - $J_2$  chain, but in the *ferromagnetic* regime. We establish that the vicinity to criticality only marginally affects the dispersion and coherence of the elementary spin-wave-like magnetic excitations, but instead results in a dramatic  $T$ -dependence of high-energy Zhang-Rice singlet excitation intensities.

PACS numbers: 75.30.Ds, 78.70.Nx, 74.72.Jt

Frustrated low-dimensional magnets serve as breeding grounds for novel and exotic quantum many-body effects. Ca<sub>2</sub>Y<sub>2</sub>Cu<sub>5</sub>O<sub>10</sub> (CYCO) and the closely related Li<sub>2</sub>CuO<sub>2</sub> (LCO) are considered candidates for this type of unconventional and challenging physics [1, 2]. These systems are in the family of frustrated edge-shared chain cuprates (ESC) and their magnetic excitation spectra, as probed by inelastic neutron scattering (INS), indicate striking puzzles. It was claimed that the dispersion of the magnetic excitations in CYCO shows an anomalous *double* branch [1, 2] while LCO exhibits a single, but weakly dispersing mode[3]. These observations would point at a strong deviation of the dispersion from standard linear spin wave theory (LSWT), in any realistic ESC parameter regime. This motivates scenarios with more sophisticated many-body physics, e.g. due to the presence of anti-ferromagnetic (AFM) interchain couplings (IC), causing the branch doubling in CYCO [1, 2]. However, such a scenario invoking strong quantum effects seems to be at odds with the observed large and almost saturated magnetic moments  $\sim 0.9\mu_B$  at  $T \ll T_N = 29.5$  K [4, 5], which suggests strongly *suppressed* quantum fluctuations. To resolve the situation it is essential to identify the precise values of the exchange interactions in these ESC's, both within and between the spin chains. To this end it is key to measure and at the same time calculate the elementary magnetic excitations, ideally for directions of momentum transfer in which the excitations depend most sensitively on the strength of the in-chain couplings. From scattering along the  $a$ -axis of CYCO, which does *not* fulfill the latter condition, a moderate value of the ferromagnetic (FM) nearest neighbor (NN) coupling  $J_1 \approx -93$  K has been extracted [1] with a tiny frustrating AFM next-nearest neighbor (NNN) exchange  $J_2 \approx 4.7$  K (see Fig.

1). From a theoretical point of view this is rather unexpected for the ESC chain geometry due to the presence of sizable O-O  $2p$  hopping along the chains. A recent reassessment of the exchange strengths based on INS on isotopically clean <sup>7</sup>Li<sub>2</sub>CuO<sub>2</sub> [6] has revealed a relatively large FM coupling  $|J_1| > 200$  K, which is more than a factor 2 larger than earlier theoretical values [7]. Given the structural similarities to CYCO, one expects a larger value  $J_1$  here too. In fact, high- $T$  <sup>89</sup>Y-NMR data on CYCO appear difficult to reconcile with small  $|J_1|$ 's [8]. Here we show that indeed by measuring with INS the magnetic excitations in CYCO along  $\mathbf{Q} = (H, 0, 1.5)$ , a direction where they are little affected by inter-chain couplings, one extracts a substantial in-chain  $J_1 \approx -170$  K and a frustrating  $J_2 \approx 32$  K, so that  $\alpha = |J_2/J_1| \approx 0.19$ . This indicates an exceptional position of CYCO within the ESC family: close to the critical point (CP) of the  $J_1$ - $J_2$  model  $\alpha_c = 1/4$ , but on the FM side of its phase diagram and in contrast with Li<sub>2</sub>ZrCuO<sub>4</sub> ( $\alpha = 0.3$  [9]) and LCO ( $\alpha = 0.33$  [6]) which are on the *spiral* side of the

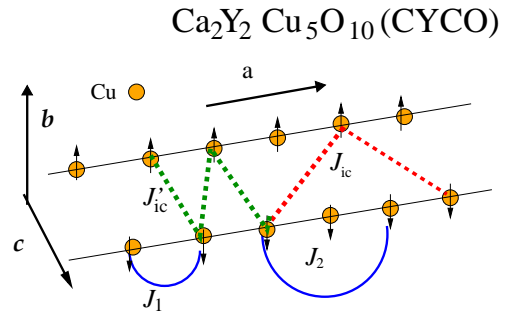


Figure 1: (Color) Schematic view of the structure of the CuO<sub>2</sub> chain layer and the main exchange paths of CYCO (see text).

critical point. We compare the obtained  $J$ 's to a realistic 5-band extended Hubbard  $pd$  model and L(S)DA+ $U$  calculations, which are in good agreement. The resulting magnetic excitations calculated with exact diagonalization compare well to the ones obtained with LSWT, implying that the coherence of the elementary, spin-wave like, magnetic excitations are marginally affected by  $\alpha$  and quantum fluctuations. However, the relatively large  $J_1$  and  $\alpha$  values obtained affect the thermodynamics [10]. The vicinity to the critical point is probed by  $\varepsilon = \alpha - \alpha_c$  strongly affects both the magnitude and de- or increasing  $T$ -dependence of the Zhang-Rice singlet (ZRS) excitation intensity for  $\varepsilon > 0$  and  $\varepsilon < 0$ , respectively. This is manifested in resonant inelastic x-ray scattering (RIXS), EELS, and optics [11] measurements as we will show.

CYCO has edge-shared  $\text{CuO}_2$  chains along the  $a$ -axis. The  $\text{Cu}^{2+}$  spins are aligned FM along the  $a$ -axis (see Fig. 1).  $ac$ -planes with  $\text{CuO}_2$  chains alternate along the  $b$ -axis with magnetically inactive cationic planes containing incommensurate and partially disordered CaY-chains which produce a non-ideal geometry in the  $\text{CuO}_2$  chains. These mutual structural peculiarities might be responsible for the puzzling strong damping at large transferred neutron momenta [1, 2] to be addressed elsewhere.

Our INS-study has been performed with a fixed final neutron energy of 14.7 meV on a 3-axis neutron spectrometer TAS-2 installed at the JRR-3 by the Japan Atomic Energy Agency. To analyze the dispersion of the magnetic excitations we adopt the model given in Ref. 1. Then, CYCO has the following main couplings  $J(\mathbf{R})$ ,  $\mathbf{R} \equiv (xa, yb, zc)$ : NN and NNN couplings along the chain  $J(1, 0, 0) \equiv J_1$ ,  $J(2, 0, 0) \equiv J_2$ , and the interchain coupling (IC)  $J(0.5, 0, 0.5) \equiv J'_{ic}$ ,  $J(1.5, 0, 0.5) \equiv J_{ic}$ ,  $J(0, 1, 0) \equiv J_b = -0.06$  meV, and  $J(0.5, 0.5, 0) \equiv J_{ab} = -0.03$  meV. For the small interplane FM couplings  $J_b$  and  $J_{ab}$  we adopt the values from Ref. 1. Their contribution to the inchain dispersion is negligible. Within the LSWT the magnetic excitations dispersion is given by Eq. (2) of Ref. 1:  $\omega^2(\mathbf{q}) = A_{\mathbf{q}}^2 - B_{\mathbf{q}}^2$ ,  $A_{\mathbf{q}} \equiv J_{\mathbf{q}} - J_0 + \tilde{J}_0 - D$ ,  $B_{\mathbf{q}} \equiv \tilde{J}_{\mathbf{q}}$ , where  $J_{\mathbf{q}} = (1/2) \sum_{\mathbf{r}} J_{\mathbf{r}} \exp(i\mathbf{q} \cdot \mathbf{r})$  is the Fourier transform of intrasublattice interactions and analogously for the intersublattice interactions  $\tilde{J}_{\mathbf{q}}$ . The dispersion along  $(0, 0, L)$  shown in Fig. 3 (c) of Ref. 1 depends only on  $J_s = J'_{ic} + J_{ic}$ . Its value, as well as the anisotropy parameter  $D$ , may be found from the INS data for  $\mathbf{q} = (0, 0, 0)$ ,  $(0, 0, 1.5)$ :  $J_s^2 = \frac{1}{4} [\omega^2(0, 0, 1.5) - \omega^2(0, 0, 0)]$ ,  $D = 2J_s - \omega(0, 0, 1.5)$ . Using  $\omega(0, 0, 1.5) = 5.03 \pm 0.03$ , and  $\omega(0, 0, 0) = 1.63 \pm 0.01$  meV we obtain  $J_s \approx 2.35$  meV, and  $D \approx -0.27$  meV [12] which is very close to  $J_s = 2.24$  meV, and  $D = -0.26$  meV found in Ref. 1. The dispersion along the line  $(H, 0, 1.5)$  depends only on the inchain  $J$ 's (if the tiny interplane  $J_{ab} = -0.03$  meV is ignored). It reads  $\omega(\mathbf{q}) = A_{\mathbf{q}} = J_{\mathbf{q}} - J_0 + \omega(0, 0, 1.5)$ . These  $J$ 's may be accessed from the dispersion along this line with much higher precision than from the previously

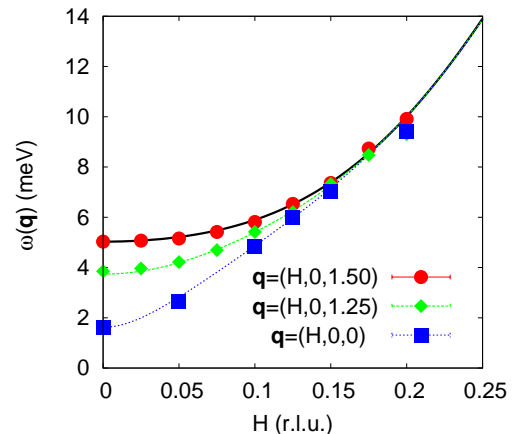


Figure 2: (Color online) Dispersion along three lines of the first Brillouin zone parallel to the  $a$ -axis, obtained from constant  $\mathbf{q}$  scans. The LSWT-fit was refined only for the dispersion along  $(H, 0, 1.5)$  and it is shown by thin lines.

reported data along  $(H, 0, 0)$  and we have [12]:

$$J_1 = -14.69 \pm 0.5 \text{ (4\%)} \text{ meV} \approx -170.4 \text{ K}, \quad (1)$$

$$J_2 = 2.78 \pm 0.2 \text{ (7.6\%)} \text{ meV} \approx 32.2 \text{ K}. \quad (2)$$

The dispersions along  $(H, 0, 0)$  (reported in Ref. 1) and  $(H, 0, 1.25)$  (given here) are affected by  $J'_{ic}$  and  $J_{ic}$ . As we have determined only their sum, we adopt  $J'_{ic}/J_{ic} = \tau \approx 4/9$  for the sake of concreteness (suggested by our band structure calculations). Notice that our  $\tau$ -value differs from 2 adopted in Ref. 1. It might be refined empirically, if one measures also along  $(H=1/6, K, L)$  for any  $K$  value.

With the aim to detect quantum effects beyond the LSWT, we calculated the dynamical structure factor  $S(\omega, q)$  using exact diagonalizations (see Fig. 3). In Fig. 2 the INS data together with the refined new LSWT-fit are shown.  $S(\omega, q)$  for our set and that of Ref. 1 are shown in Fig. 3. The peak positions always nicely follow the LSWT-curves, however our set gives a better description of the INS-data than that in Ref. 1 (Fig. 4 therein) where the artificial double branching was ascribed to AFM IC. Indeed, it induces some intensity apart from the LSWT-curve, but these intensities are far too weak to be considered as a branch doubling. Notice the inflection point at  $\pi/2$  for finite  $\alpha$ . The total dispersion width is given solely by  $2|J_1|$ .

As an application of our data, we consider the 1D-magnetic susceptibility  $\chi(T)$  in the isotropic limit (see Fig. 4). Despite the uncertainty caused by the unknown background susceptibility  $\chi_0$ , the relatively large value of  $|J_1|$  doesn't allow to extract directly  $\Theta_{CW}$  from a  $1/\chi(T)$  plot using only data up to 300 K. Instead a much broader  $T$ -interval up to about 800 K would be required to reach the asymptotic high- $T$  limit necessary for a proper quasi-linear behavior. Alternatively, higher orders in the high- $T$  expansion can be applied [13]. Hence, the reported

AFM values  $\Theta_{CW} \sim -15$  K [14] or weak FM ones  $\Theta_{CW} \sim +8$  K [15] are rather artificial. Using the  $J$ 's from our INS-fits we predict instead a markedly larger FM value

$$\Theta_{CW} = 0.5(|J_1| - J_2) - J'_{ic} - J_{ic} - J_{ab} = +43.4 \text{ K}. \quad (3)$$

Since we found  $\alpha < \alpha_c$ , we readily predict the value of the 2D saturation field  $H_s$  which is here determined solely by the total AFM IC like for LCO [16]:  $gH_s = 4(J'_{ic} + J_{ic}) = \frac{2}{g}77.4 \text{ T} \approx 64.8 \text{ T}$ , refining an estimate of 70 T for  $H \parallel b$  and  $g = 2.39$  from low-field magnetization data [15]. Next we consider the magnetic moment in the ordered state at low  $T$ . Within the LSWT the reduction due-to quantum fluctuations is about 6.8% which yields  $1.07\mu_B$  to be compared with the experimental value of  $0.92 \pm 0.08\mu_B$  [5] which however is affected by the chemical reduction effect since about  $0.22 \pm 0.04$  of the local moment resides on the O  $2p$  orbitals.

The exchange coupling strengths can also be determined by DFT+ $U$  calculations. For this we used the full potential scheme FPLO [17] (vers. fplo9.01) and performed super cell calculations for different collinear spin arrangements applying LDA and GGA functionals [18, 19]. The Coulomb repulsion  $U_{3d}$  was varied in the physical relevant range from 5 to 8 eV for a fixed  $J_{3d} = 1$  eV. In our calculations the incommensurate crystal structure of CYCO can be treated only approximately. Thus, we neglect (i) the modulation of the Cu-O distances within the  $\text{CuO}_2$  chains and its buckling and (ii) the incommensurability of the  $\text{CuO}_2$  and the CaY subsystems. In particular, the  $\text{CuO}_2$  chains were treated as ideal planar chains reflecting an averaged Cu-O distance of 1.92 Å and a Cu-O-Cu bond angle of  $94.5^\circ$ . Furthermore, we modelled the CaY layer by a Na layer to preserve the half filling of the system. The structure of the simplified model systems is given in Ref. 20. These structural simplifications allow a reliable modelling of  $J_1$  yielding an FM value:  $\sim -150$  K [20]. In previous studies

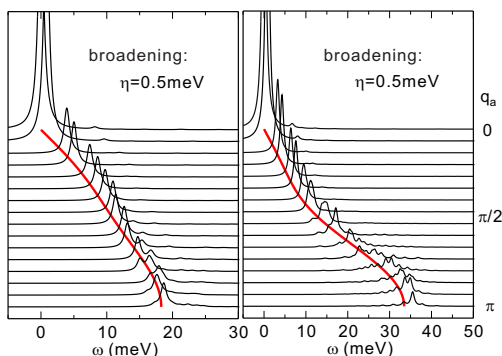


Figure 3: (Color) Magnetic dynamical structure factor  $S(\omega, q)$  for the  $J$ -set of Ref. 2 (left) and for our set (right) from exact diagonalizations with  $L = 14 \times 2$  and  $15 \times 2$  adopting  $\tau = D = 0$  and  $J_{ic} = 2.24$  meV, (see Ref. 16. Red line: dispersion from LSWT for the two parameter sets (see Fig. 2 and text).

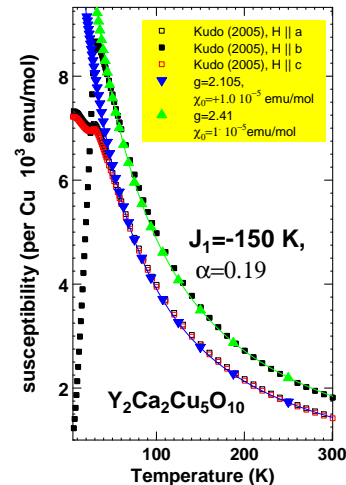


Figure 4: (Color) Spin susceptibility  $\chi(T)$  within the isotropic 1D  $J_1$ - $J_2$  model using the transfer matrix renormalization group method,  $\chi_0$  - background susceptibility.

of closely related ESC [21, 22] for the effects of (i) chain buckling and (ii) the cation related crystal fields it was shown that  $J_1$  is rather robust whereas  $J_2$  is strongly reduced by a factor 2 to 3. Thus, our  $-J_1 \sim 150$  K is considered as a rather reliable lower estimate by about 10 to 20% with respect to the buckled chain geometry in CYCO. However, in view of the drastic dependence of  $J_2$  on these parameters [21, 22], a derivation of a reliable value from the applied model structure is difficult. Thus, CYCO fits the general experience of a sizable FM  $J_1$ -value for ESC in contrast to the assignments of only a few K, proposed for  $\text{LiVCuO}_4$  [23] and  $\text{NaCu}_2\text{O}_2$  [24]. Such small  $J_1$ 's would put them in a region of strong quantum fluctuations, harboring the difficulty that the observed pitch angle cannot be described classically [25].

Whereas the vicinity of CYCO to the quantum critical point only weakly affects the dispersion and coherence of the elementary, spin-wave like, magnetic excitations, we will show that the amplitude to excite Zhang-Rice singlets (ZRS) at typical high-energies, probed by spectroscopic means depends strongly on the frustrating  $J_2$  and temperature. We have also performed exact diagonalization calculations using an extended 5-band Cu  $3d$   $\text{O}2p$  Hubbard model for CYCO with a standard parameters [28]. To fit the INS-derived value of  $J_2 = 32$  K, the  $t_{px,px} = 0.59$  eV has been slightly reduced as compared with LCO (0.84 eV,  $J_2 = 76$  to 66 K) which simulates probably the deviations from the ideal chain geometry. Mapping the spin states of the 5-band Hubbard model onto a frustrated spin model, we obtain  $J_1 = -177.5$  K and  $J_2 = 32.3$  K in full accord with the LSWT-analysis of the INS data given above. We stress that the value of  $J_1$  is mainly determined by the direct FM exchange cou-

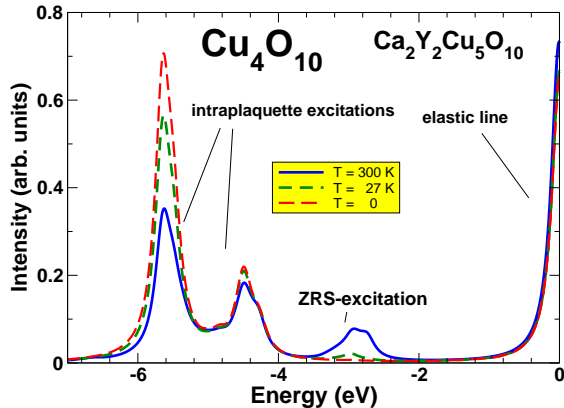


Figure 5: (Color)  $T$ -dependent O-K RIXS-spectrum for  $xx$ -polarization from a  $\text{Cu}_4\text{O}_{10}$  cluster within exact diagonalization using a Lorentzian broadening (half width  $\Gamma = 0.13$  eV).

pling  $K_{pd} = 65$  meV and not by the Hund's rule coupling on the O sites  $J_p = 0.5 (U_p - U_{p_x p_y}) = 0.6$  eV as often adopted. The significant value of  $J_1$  is generic for ESC with a Cu-O-Cu bond angle  $\varphi < 96^\circ$  at variance from the case of  $\text{CuGeO}_3$  with  $\varphi \approx 98^\circ$  causing an AFM  $J_1$ .

As a modern spectroscopy, RIXS provides valuable insights into the correlated orbital and electronic structure (for a review see Ref. 26). Therefore, we also studied the  $T$ -dependent O-K edge RIXS-spectra for a  $\text{Cu}_4\text{O}_{10}$  cluster within exact diagonalization (see Fig. 5). We find a strong *decrease* of the intensity for the ZRS excitons with decreasing  $T$ , which is qualitatively in accord with general considerations for EELS and optics [11]. The not yet assigned feature observed for CYCO at 300 K near 527 eV (Fig. 5 in Ref. 27, counted from the 530 eV excitation energy) corresponds just to these excitations. It perfectly agrees with 2.95 eV obtained here. Notice that when one sets  $t_{p_x, p_x} = 0$ , thereby strongly suppressing  $J_2 \propto t_{p_x, p_x}^2$ , no ZRS exciton is observed even at 300 K. Hence, the frustrated FM differs qualitatively from a pure FM in its high-energy response.

To summarize, we have shown that  $\text{Ca}_2\text{Y}_2\text{Cu}_5\text{O}_{10}$  is a frustrated quasi-1D ferromagnet close to criticality. This edge-sharing spin-chain compound has pronounced FM correlations in the presence of a sizable in-chain frustration. The main intensity of magnetic excitations in  $S(\omega, q)$  is reasonably well described within LSWT. The signatures of the sizable in-chain frustration found here cause (i) a characteristic curvature of the in-chain dispersion of magnetic excitations and (ii) Zhang-Rice singlet features at  $\sim 3$  eV that are strongly  $T$ -dependent and are detectable by spectroscopies. The spin alignment between the chains below  $T_N$  is supported by a specific AFM inter-chain coupling which determines the saturation field. It causes interesting quantum effects that go beyond a linear spin wave description. These

effects, and the interplay of  $J'_{ic}$  and  $J_{ic}$ , provide an interesting problem not yet investigated in full detail. However, such quantum effects are neither strong enough to cause a breakdown of LSWT, nor to induce an additional branch of magnetic excitations, as suggested previously. Our results can further aid in the correct assignment of the frustration [23, 24] in other ESC, including multiferroics, but especially for the complex chain-ladder system  $(\text{La, Sr, Ca})_{14}\text{Cu}_{24}\text{O}_{41}$  [29] which also possibly contains frustrated FM  $\text{CuO}_2$  chains as suggested by the edge-sharing geometry and sizable NNN transfer integrals [30] giving rise to significant AFM  $J_2$ 's. Its nonideal chains, as with CYCO, challenge one to look for more sophisticated but yet solvable theoretical models that include incommensurate and disorder effects.

We thank the DFG for financial support. In particular, the Emmy-Noether program is acknowledged for founding. We also acknowledge fruitful discussions with J. Richter, J. Geck, and V. Bisogni.

\* Corr. author, E-mail: s.l.drechsler@ifw-dresden.de

- [1] M. Matsuda *et al.*, Phys.Rev.B, **63**, 180403 (2001).
- [2] M. Matsuda *et al.* J. Phys. Soc. Jpn. **74**, 1578 (2005).
- [3] M. Boehm *et al.*, EPL **43**, 77 (1998).
- [4] M. Matsuda *et al.* J. Phys. Soc. Jpn. **68**, 269 (1999).
- [5] H.F. Fong *et al.*, Phys. Rev. B **59** 6873 (1999).
- [6] W.E.A. Lorenz *et al.*, EPL **88** 37002 (2009).
- [7] Y. Mizuno *et al.* Phys. Rev. B **57**, 5326 (1998).
- [8] H.-J. Choi *et al.*, Low Temp. Phys., Parts A & B (Ed. Y. Takano) Book Ser.: AIP Conf. Proc. **850**, 1019 (2006).
- [9] S.-L. Drechsler *et al.*, Phys. Rev. Lett. **98**, 077202 (2007).
- [10] M. Härtel *et al.* Phys. Rev. B **84**, 104411 (2011).
- [11] J. Málek *et al.*, Phys. Rev. B **78**, 060508(R) (2008).
- [12] These  $J$ 's belong to a fit including both const.  $E$  and  $\mathbf{q}$ -scans. A fit with const.  $\mathbf{q}$  scans, only, yields close values:  $J_1 = -164.9$  K (5.95%),  $J_2 = 31.1$  K for  $J_3 = 0$  fixed and  $D = -3.1$  K, i.e.  $\alpha \approx 0.19$ .
- [13] H.-J. Schmidt *et al.*, Phys. Rev. B **84**, 104443 (2011).
- [14] H. Yamaguchi *et al.*, Physica C **320**, 167 (1999).
- [15] K. Kudo *et al.*, Phys. Rev. B **71**, 104413 (2005).
- [16] S. Nishimoto *et al.*, Phys. Rev. Lett. **107** 097201 (2011).
- [17] K. Koepnik *et al.* Phys. Rev. B **59**, 1743 (1999).
- [18] P. Perdew *et al.* Phys. Rev. B **45**, 13244 (1992).
- [19] P. Perdew *et al.*, Phys. Rev. Lett. **77**, 3865 (1997).
- [20] See EPAPS Document No. []. For more information on EPAPS, see <http://www.aip.org/pubservs/epaps.html>
- [21] M. Schmitt *et al.*, Phys. Rev. B **80**, 205111 (2009).
- [22] M. Schmitt *et al.* to be published.
- [23] M. Enderle *et al.*, EPL (2005).
- [24] L. Capogna *et al.*, Phys. Rev. B **71** 140402 (2005)
- [25] S. Nishimoto *et al.*, EPL submitted (arXiv:1105.2810v2)
- [26] L. Ament *et al.*, Rev. Mod. Phys. **83**, 705 (2011).
- [27] E. Kabasawa *et al.*, J. ESRP, **148**, 55 (2005).
- [28] We used  $U_d = 8.5$  eV,  $U_p = 4.1$  eV, the interorbital on-site Coulomb repulsion on O sites  $U_{p_x p_y} = 2.9$  eV, charge transfer energies  $\Delta_{p_x d} = 3.5$  eV, and  $\Delta_{p_y d} = 3.8$  eV (close to Ref. 7 with an isotropic value  $\Delta_{pd} = 3.8$  eV). We further include the intersite Coulomb interaction



$V_{pd} = 0.5$  eV neglected in Ref. 7. This seems to be the main reason for the difference of the ZRS-exciton energies, upshifted by  $\sim 0.3$  eV compared to Ref. 7.

[29] S.A. Carter *et al.*, Phys. Rev. Lett. **77**, 1378 (1996).

[30] U. Schwingenschlögl *et al.* Eur. Phys. J. B **55**, 43 (2007).

---

## EPAPS supplementary online material:

### " $\text{Ca}_2\text{Y}_2\text{Cu}_5\text{O}_{10}$ : the first frustrated quasi-1D ferromagnet close to criticality "

R.O. Kuzian, S. Nishimoto, S.-L. Drechsler, J. Málek, J. van den Brink

IFW Dresden, P.O. Box 270116, D-01171 Dresden, Germany

M. Schmitt, and H. Rosner

Max-Planck Institute for Chemical Physics of Solids, 01187 Dresden, Dresden, Germany

M. Matsuda,

Quantum Condensed Matter Division, Oak Ridge National Laboratory, Oak Ridge, TN 37831, USA

K. Oka, H. Yamaguchi and T. Ito

AIST, Tsukuba, Ibaraki 305-8562, Japan

In the present EPAPS supplementary online material we present (i) exact diagonalization studies of the dynamical structure factor for coupled chains with various interchain couplings of the type as realized in CYCO. (ii) We show our prediction and details of the calculated optical conductivity  $\sigma(\omega)$  (iii) We demonstrate the influence of interchain coupling and spin anisotropy on the magnetic susceptibility. (iv) we provide the reader with further details of the LSDA+ $U$  and GGA+ $U$  calculations. (v) we illustrate the influence of inchain frustration on the dispersion of magnetic excitations focussing on its curvature behavior and in particular on the positions of inflection points within linear spin-wave theory.

### The spin-Hamiltonian with uniaxial anisotropy and CYCO geometry

In general, spin waves are the quanta of small oscillations of spins around the classical ground state of the spin-Hamiltonian. So, for the same Hamiltonian, the form of the dispersion may be radically different for different values of parameters, since the classical ground state may be different from the quantum one. The spin-Hamiltonian for CYCO reads

$$\hat{H} = \hat{H}_A + \hat{H}_B + \hat{H}_{AB} \quad (\text{S1})$$

$$\begin{aligned} \hat{H}_{A(B)} = & \frac{1}{2} \sum_{\mathbf{m} \in A(B)} \left\{ \sum_{\mathbf{r}} \left[ J_{\mathbf{r}}^z \hat{S}_{\mathbf{m}}^z \hat{S}_{\mathbf{m}+\mathbf{r}}^z + J_{\mathbf{r}} \hat{S}_{\mathbf{m}}^+ \hat{S}_{\mathbf{m}+\mathbf{r}}^- \right] \right. \\ & \left. + \sum_{\mathbf{R}} \left[ J_{\mathbf{R}}^z \hat{S}_{\mathbf{m}}^z \hat{S}_{\mathbf{m}+\mathbf{R}}^z + J_{\mathbf{R}} \hat{S}_{\mathbf{m}}^+ \hat{S}_{\mathbf{m}+\mathbf{R}}^- \right] \right\} \quad (\text{S2}) \end{aligned}$$

$$\begin{aligned} \hat{H}_{AB} = & \sum_{\mathbf{m} \in A} \sum_{\mathbf{f}} \left[ \tilde{J}_{\mathbf{f}}^z \hat{S}_{\mathbf{m}}^z \hat{S}_{\mathbf{m}+\mathbf{f}}^z \right. \\ & \left. + \frac{\tilde{J}_{\mathbf{f}}}{2} \left( \hat{S}_{\mathbf{m}}^+ \hat{S}_{\mathbf{m}+\mathbf{f}}^- + \hat{S}_{\mathbf{m}}^- \hat{S}_{\mathbf{m}+\mathbf{f}}^+ \right) \right] \quad (\text{S3}) \end{aligned}$$

where  $\mathbf{m}$  enumerates the sites in one sublattice, ( $\mathbf{r} = \pm n\mathbf{a}$ ,  $n = 1, 2, \dots$ ) determines the neighboring sites within the chain,  $\mathbf{a}$  being the lattice vector along the chain, vector  $\mathbf{f}$  connects the sites of different chains in the  $\mathbf{ac}$  plane,  $\mathbf{R}$  connects the sites in different planes, but in the same sublattice in CYCO. We have allowed for an uniaxial anisotropy of the exchange interactions.

### Linear spin-wave theory

For the collinear AFM the classical ground state is the Néel state, the spins on the  $A$  sublattice are directed up, and down in the  $B$  sublattice. We introduce two different sets of spin-deviation operators

$$\hat{S}_{\mathbf{m} \in A}^+ \equiv \sqrt{2S} f_{\mathbf{m}}(S) a, \quad \hat{S}^- \equiv \sqrt{2S} a^\dagger f_{\mathbf{m}}(S), \quad (\text{S4})$$

$$\hat{S}^z \equiv S - \hat{n}_{\mathbf{m}}, \quad \hat{n}_{\mathbf{m} \in A} = a_{\mathbf{m}}^\dagger a_{\mathbf{m}} \quad (\text{S5})$$

$$\hat{S}_{\mathbf{m} \in B}^- \equiv \sqrt{2S} f_{\mathbf{m}}(S) b, \quad \hat{S}^+ \equiv \sqrt{2S} b^\dagger f_{\mathbf{m}}(S), \quad (\text{S6})$$

$$\hat{S}^z \equiv -S + \hat{n}_{\mathbf{m}}, \quad \hat{n}_{\mathbf{m} \in B} = b_{\mathbf{m}}^\dagger b_{\mathbf{m}}, \quad (\text{S7})$$

$$f_{\mathbf{m}}(S) = \sqrt{1 - \hat{n}_{\mathbf{m}}/2S} \quad (\text{S8})$$

$$= 1 - (\hat{n}_{\mathbf{m}}/4S) - \frac{1}{32} (\hat{n}_{\mathbf{m}}/S)^2 + \dots \quad (\text{S9})$$

The Néel state (AFM ordering of FM chains in the  $\mathbf{ac}$  plane) is the vacuum state for the operators  $b$  |Neel> = 0. So, the operator  $b(a)$  annihilates the spin deviation from the Néel order (which means a spin-flip for  $s = 1/2$ ) on the sublattice  $B(A)$ . The Hamiltonian (S1) can be rewritten as

$$\hat{H} = \hat{H}_0 + \hat{H}_{int}, \quad (\text{S10})$$

$$\begin{aligned} \hat{H}_0 = & \sum_{\mathbf{q}} [A_{\mathbf{q}} (a_{\mathbf{q}}^\dagger a_{\mathbf{q}} + b_{\mathbf{q}}^\dagger b_{\mathbf{q}}) \\ & + B_{\mathbf{q}} (a_{\mathbf{q}} b_{-\mathbf{q}} + a_{\mathbf{q}}^\dagger b_{-\mathbf{q}}^\dagger)], \end{aligned} \quad (\text{S11})$$

$$A_{\mathbf{q}} \equiv S \left[ \sum_{\mathbf{r}, \mathbf{R}} J_{\mathbf{r}} \exp(i\mathbf{q}\mathbf{r}) - \sum_{\mathbf{r}, \mathbf{R}} J_{\mathbf{r}}^z + \sum_{\mathbf{f}} \tilde{J}_{\mathbf{f}}^z \right], \quad (\text{S12})$$

$$B_{\mathbf{q}} \equiv S \sum_{\mathbf{f}} I_{\mathbf{f}} \exp(i\mathbf{q}\mathbf{f}) \quad . \quad (\text{S13})$$

The Fourier transform of e.g.  $b_{\mathbf{q}}$  reads  $b_{\mathbf{q}} = \sqrt{2/N} \sum_{\mathbf{m} \in B} \exp(-i\mathbf{q}\mathbf{m}) b_{\mathbf{m}}$ ;  $N$  denotes the total number of sites. The transverse part of  $\hat{H}$  (S1) defines the one-particle hoppings in  $\hat{H}_0$  (S11), the Ising part contributes on-site energy values. The terms, which contain more than two spin-wave operators enter  $\hat{H}_{int}$ . The magnons  $\alpha_{\mathbf{q}}, \beta_{\mathbf{q}}$  in an AFM are introduced as a mean-field solution of Eq. (S10) [? ], which *neglects*  $\hat{H}_{int}$ .

$$[\alpha_{\mathbf{q}}, \hat{H}] \approx \omega_{\mathbf{q}} \alpha_{\mathbf{q}}, \quad [\beta_{\mathbf{q}}, \hat{H}] \approx \omega_{\mathbf{q}} \beta_{\mathbf{q}} \quad (\text{S14})$$

$$\omega_{\mathbf{q}} = \sqrt{A_{\mathbf{q}}^2 - B_{\mathbf{q}}^2}, \quad (\text{S15})$$

$$\alpha_{\mathbf{q}} = \cosh \theta_{\mathbf{q}} a_{\mathbf{q}} + \sinh \theta_{\mathbf{q}} b_{-\mathbf{q}}^\dagger, \quad (\text{S16})$$

$$\beta_{\mathbf{q}} = \cosh \theta_{\mathbf{q}} b_{-\mathbf{q}} + \sinh \theta_{\mathbf{q}} a_{\mathbf{q}}^\dagger$$

$$\tanh 2\theta_{\mathbf{q}} = B_{\mathbf{q}}/A_{\mathbf{q}}.$$

Now we specify the expressions for  $A_{\mathbf{q}}, B_{\mathbf{q}}$ , which result from the geometry of CYCO and the spin value  $s = 1/2$ . In the summations over  $\mathbf{r}, \mathbf{R}, \mathbf{f}$  we retain only the following terms. For the in-chain exchanges we retain  $J_1, J_2$ , which correspond to  $\mathbf{r} = \mathbf{a}, 2\mathbf{a}$ , respectively. For the interchain interactions we retain  $J'_{ic}, J_{ic}, J_b, J_{ab}$ , which correspond to  $\mathbf{f}' = (\mathbf{a} + \mathbf{c})/2, \mathbf{f} = (3\mathbf{a} + \mathbf{c})/2, \mathbf{R}_b = \mathbf{b}, \mathbf{R}_{ab} = (\mathbf{a} + \mathbf{b})/2$ . Then we find

$$\begin{aligned} A_{\mathbf{q}} = & J_1 (\cos q_a a - 1) + J_2, (\cos 2q_a a - 1) \\ & + J_b (\cos q_b b - 1) + \\ & + 2J_{ab} \left( \cos \frac{q_a a}{2} \cos \frac{q_b b}{2} - 1 \right) + 2J_s - D, \end{aligned} \quad (\text{S17})$$

$$B_{\mathbf{q}} = 2 \left[ J'_{ic} \cos \frac{q_a a}{2} + J_{ic} \cos \frac{3q_a a}{2} \right] \cos \left( \frac{q_c c}{2} \right). \quad (\text{S18})$$

Note that interplane interactions enter  $A_{\mathbf{q}}$  as they represent intra-sublattice interactions. The value of the gap at  $\mathbf{q} = 0$  is

$$\Delta = \sqrt{A_0^2 - B_0^2}, \quad (\text{S19})$$

the anisotropy enters the dispersion via the integral value  $D$ , which is defined as

$$A_0 - B_0 \equiv D = \sum_{\mathbf{f}} (\tilde{J}_{\mathbf{f}}^z - \tilde{J}_{\mathbf{f}}) - \sum_{\mathbf{r}, \mathbf{R}} (J_{\mathbf{r}}^z - J_{\mathbf{r}}), \quad (\text{S20})$$

and is related to the gap value by the relations

$$\begin{aligned} \Delta &= \sqrt{D(D + 2B_0)}, \\ D &= \left( \sqrt{B_0^2 + \Delta^2} - B_0 \right). \end{aligned} \quad (\text{S21})$$

### Dispersion of magnetic excitations and inchain frustration

Ignoring tiny interactions like  $J_b$  for  $qc = 2(m+1)\pi$ ,  $m = 0, 1, 2, \dots$  the dispersion along (H,0,1.5) within the LSWT reads (see Eq. 2 in Ref. 1):

$$\begin{aligned} \frac{\omega}{|J_1|} &= 1 - \cos x + \alpha (\cos 2x - 1) + \\ &2\beta + \gamma (\cos 3x - 1) + \dots, \end{aligned} \quad (\text{S22})$$

where  $x = qa$ ,  $\gamma = J_3 / |J_1|$  denotes the third neighbor inchain coupling. The dimensionless interchain coupling constant slightly "renormalized" by the anisotropy parameter  $D$ :  $\beta_D = (J_s - 0.5D) / |J_1| \approx 0.17$  has been omitted in Fig. S1 since it doesn't affect the curvature of the dispersion curve in the case under consideration. According to our results of the mapping of the 5-band extended Hubbard  $pd$ -model on a frustrated spin model  $\gamma$  is usually FM but very small  $\sim 10^{-2}$  to  $10^{-3}$ . In many cases it can be therefore neglected. The whole width of the dispersion  $W$  is given by the odd Fourier coefficients, only:  $W = 2(|J_1| + J_3 + \dots)$ . In the limit  $x \ll 1$  Eq. (S22) can be rewritten as

$$\frac{\omega}{|J_1|} - 2\beta \approx \frac{1 - 4\alpha - 9\gamma}{2} x^2 - \frac{1 - 16\alpha - 81\gamma}{24} x^4 + O(x^6). \quad (\text{S23})$$

Thus, the inchain frustration  $\alpha > 0$  reduces the quadratic term (which vanishes approaching the critical point, see Fig. S1) and strongly affects the quartic term which is *negative* for the unfrustrated FM ( $\alpha = 0$ ) but changes its sign for a sizable value of  $\alpha > (1 - 81\gamma)/16 \approx 1/16$  to  $1/8$ , well realized for CYCO with  $\alpha = 0.19$ . Thus, a *positive* sign of the quartic term gives direct evidence for a pronounced frustrated ferromagnet. Just the opposite behavior is realized near the maximum of the dispersion near the BZ boundary. There the expansion in terms of  $\varepsilon = \pi - qa$  reads

$$\begin{aligned} \frac{\omega}{|J_1|} - 2\beta &\approx 2(1 - \gamma) - \frac{1 + 4\alpha - 9\gamma}{2} x^2 + \\ &+ \frac{1 + 16\alpha - 81\gamma}{24} x^4 + O(x^6), \end{aligned} \quad (\text{S24})$$

the inchain frustration  $\alpha$  enhances the negative quadratic term (see also Fig. S1) In the case  $J_3 = 0$  approximately fulfilled for almost all ELC, the inflection point  $q_{ip}$  of the dispersion curve (Eq. (S22)) is given by

$$q_{ip}a = \cos^{-1} \left( \frac{1 - \sqrt{1 + 128\alpha^2}}{16\alpha} \right). \quad (\text{S25})$$

It provides also a clear measure of the inchain frustration  $\alpha = J_2 / |J_1|$  present in the system (see Fig. S1). To summarize, analyzing the full dispersion curve along the line (H,0,1.5) the presence of the inchain frustration  $\alpha$  is easily detected.

However, we admit that in many cases where the full dispersion curve is not available, a fit of a significant part of the total curve might provide a more precise value of  $\alpha$  or  $J_2$ . In such cases the extraction of  $\alpha$  from the  $T$ -dependence of the Zhang-Rice exciton intensity shown in the main text might provide a reasonable alternative.

Now we briefly consider the (H,0,0) scattering direction where the interchain coupling (IC) is involved. Compared with the former "1D"-case we show in Fig. S2 that the IC has a sizable influence on the shape and on the curvature of the dispersion. Note that a small quadratic term exists only for finite anisotropy  $-D > 0$ .

$$\frac{\omega}{|J_1|} = \sqrt{\Delta_0^2 + \frac{1}{2}[(1-4\alpha)\beta_D + 2\beta(\beta + 8\beta_2)]x^2 + O(x^4)}, \quad (\text{S26})$$

where  $\delta = -D/|J_1|$ ,  $\beta = J_s/|J_1|$ , and  $\beta_2 = J_{ic}/|J_1|$ . In the isotropic limit  $D$  or  $\delta = 0$ , i.e. when the spin gap  $\Delta_0 = \sqrt{4\delta\beta + \delta^2}$  vanishes, the dispersion becomes linear (compare Fig. 3 (left) in the main text).

Like in the former case one observes that the in-chain frustration  $\alpha$  strongly enhances the higher order terms near the  $\Gamma$  point. But the interchain coupling reduces this enhancement. Under such circumstances the extraction of the IC and  $\alpha$  from a scattering direction affected by both types of interactions is inconvenient.

### Magnetic excitations within the model of coupled chains

We fix the sum of the two interchain couplings  $J_s = J'_{ic} + J_{ic} = 2.241$  meV at the value derived from the INS data and change only their ratio  $\tau$ . First we switch off the frustrating NNN AFM inchain coupling  $J_2$  and adopt for  $J_1$  the value suggested in Ref. 1 (see Fig. 5) One observes roughly two kinds of dispersing peaks: one with a dominant intensity well described by the LSWT and second one which much less intensity. The latter type of curves has been interpreted as "evidence" for an additional anomalous second ME branch in Refs. 1. A similar behavior is observed for all cases with a dominant NN interchain coupling  $J'_{ic}$ . In the opposite case of a dominant  $J_{ic}$  that second curve almost invisible. For our parameter set that minority peaks are much less pronounced. Thus we conclude, that this quantum effect depends on the details of the two main AFM interchain couplings and becomes weaker with increasing  $|J_1|$  in contrast to what has been suggested previously. Anyhow, a systematic study including the examination of finite size scaling is left for a future investigation since it is of less relevance for CYCO.

### The reduction of the magnetic moment at $T = 0$

In contrast to the case of FM ordering, the vacuum state for the antiferro-magnons  $\alpha_{\mathbf{q}}, \beta_{\mathbf{q}}$  (S16) does not coincide with the classical Neel ground state  $|\text{Neel}\rangle \neq |0\rangle$ . Thus, the vacuum  $|0\rangle$  contains a finite number of spin deviations (S5),(S7) even at  $T = 0$ ,  $\langle 0|\hat{n}_{\mathbf{m}}|0\rangle \neq 0$ . Expressing the spin deviation operators  $a_{\mathbf{q}}$  via  $\alpha_{\mathbf{q}}, \beta_{\mathbf{q}}$  (S16), we obtain

$$\begin{aligned} \langle 0|a_{\mathbf{m}}^\dagger a_{\mathbf{m}}|0\rangle &= \frac{2}{N} \sum_{\mathbf{q}} \langle 0|a_{\mathbf{q}}^\dagger a_{\mathbf{q}}|0\rangle \\ &= \frac{2}{N} \sum_{\mathbf{q}} \sinh^2 \theta_{\mathbf{q}} \langle 0|\beta_{\mathbf{q}}\beta_{\mathbf{q}}^\dagger|0\rangle = \frac{1}{N} \sum_{\mathbf{q}} \left( \frac{A_{\mathbf{q}}}{\omega_{\mathbf{q}}} - 1 \right). \end{aligned} \quad (\text{S27})$$

Note, that in our geometry, the summation over  $\mathbf{q}$  runs over the magnetic Brillouin zone (BZ) which in the present case coincides with the lattice BZ  $\frac{2\pi}{a} \times \frac{2\pi}{b} \times \frac{2\pi}{c}$ . Finally, for the sublattice magnetization at  $T = 0$ , we have

$$\langle 0|\hat{S}_{\mathbf{m}}^z|0\rangle = S \left( 1 - \frac{\langle 0|\hat{n}_{\mathbf{m}}|0\rangle}{S} \right). \quad (\text{S28})$$

### The optical conductivity within the 5-band extended Hubbard model

Focusing on the Zhang-Rice exciton, we note that a similar picture as in the RIXS spectra is shown in the predicted optical conductivity and EELS spectra (not shown here). Some insight in the corresponding transitions can be gained from the zoomed figure with an artificial small broadening to resolve these transitions (see Fig. S5).



site	x/a	y/b	z/c
Cu	3/8	0	1/4
Cu	7/8	0	1/4
Cu	1/8	1/2	1/4
Cu	5/8	1/2	1/4
O	3/8	0	.6270
O	7/8	0	.6270
O	1/8	1/2	.6270
O	5/8	1/2	.6270
O	3/8	0	.8730
O	7/8	0	.8730
O	1/8	1/2	.8730
O	5/8	1/2	.8730
Na	1/8	1/4	0
Na	5/8	1/4	0
Na	1/8	1/4	1/2
Na	5/8	1/4	1/2

Table S1: Crystal structure of the *commensurate* approximate effective  $\text{Na}_2\text{CuO}_2$  compound for DFT+ $U$  calculation (enlarged unit cell and reduced symmetry to allow different spin configuration). Space group P2/M (SG 10),  $a = 5.6306 \text{ \AA}$ ,  $b = 6.286 \text{ \AA}$  and  $c = 10.5775 \text{ \AA}$ .

### Additional information on the L(S)DA+ $U$ calculations

To model the mutually incommensurate crystal structure of CYCO we neglect (i) the modulation of the Cu-O distances within the  $\text{CuO}_2$  chains and (ii) the incommensurability of the  $\text{CuO}_2$  and CaY subsystems as a good approximate to estimate the NN exchange along the  $\text{CuO}_2$  chains. The crystal structure data for this simplified model structure are given in Tab. S2. To calculate the NN exchange  $J_1$  for the approximated crystal structure we constructed a super cell by the doubling of the unit cell and the reduction of its symmetry to allow for different spin configurations (see Tab. S1). The obtained FM NN exchange  $J_1$  depending on the Coulomb repulsion  $U_{3d}$  and the specific functional are depicted in Fig. S6.  $J_1$  depends only weakly on these parameters. The given NN exchange  $J_1 = -150 \text{ K}$  is the average between the LDA and GGA result at  $U_{3d} = 6.5 \text{ eV}$ .

### Aspects of the magnetic susceptibility

In addition to 1D susceptibilities, for the isotropic as well as the easy-axis anisotropic case calculated using the transfer matrix renormalization group theory method, also the 3D case has been examined treating the adopted isotropic interchain coupling (IC) within the RPA (random phase approximation) (see Fig. S7 and Eq. (S29)).

$$\chi_{3D}(T) \approx \frac{\chi_{1D}(T)}{1 + k\chi_{1D}(T)} \quad . \quad (\text{S29})$$

site	x/a	y/b	z/c
Cu	0	0	0
O	0	0	0.623
Na	1/2	1/4	1/4

Table S2: Crystal structure of the *commensurate* approximate effective  $\text{Na}_2\text{CuO}_2$  structure as a starting model for CYCO. Space group FMMM (SG 69),  $a = 2.8153 \text{ \AA}$ ,  $b = 6.286 \text{ \AA}$  and  $c = 10.5775 \text{ \AA}$ .

- [1] M. Matsuda *et al.*, Phys. Rev. B, **63**, 180403 (2001).
  - [2] T. Oguchi, Phys. Rev. **117**, 117 (1960).
-

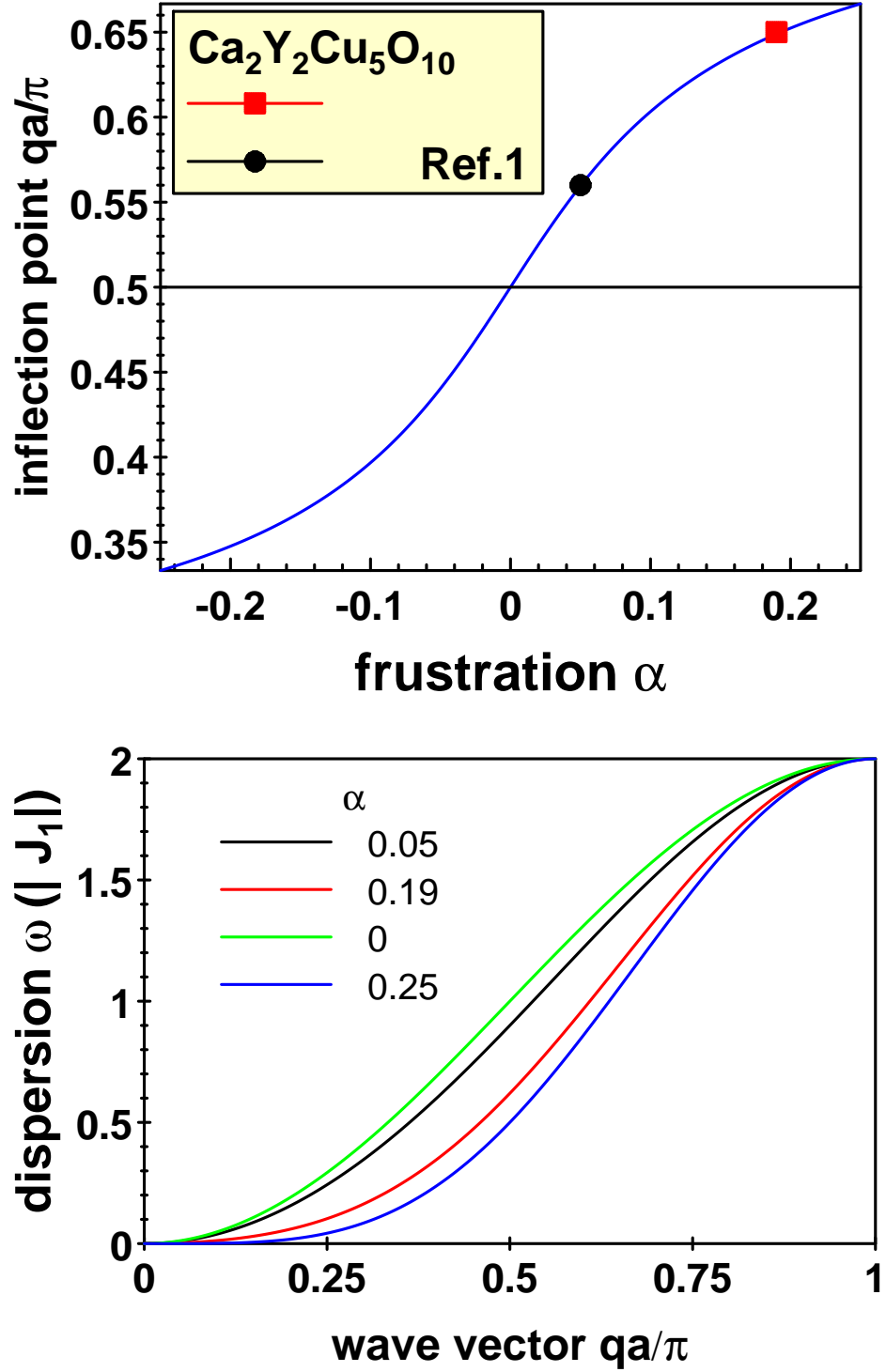


Figure S1: (Color) The influence of the frustration  $\alpha$  on the dispersion of magnetic excitation for a direction not affected by the interchain coupling, e.g. (H,0,1.5) (see Fig. 2 of the main text). Uper: position of the inflection point. Blue curve Eq. (S25). lower: the full dispersion for various  $\alpha$ -values.

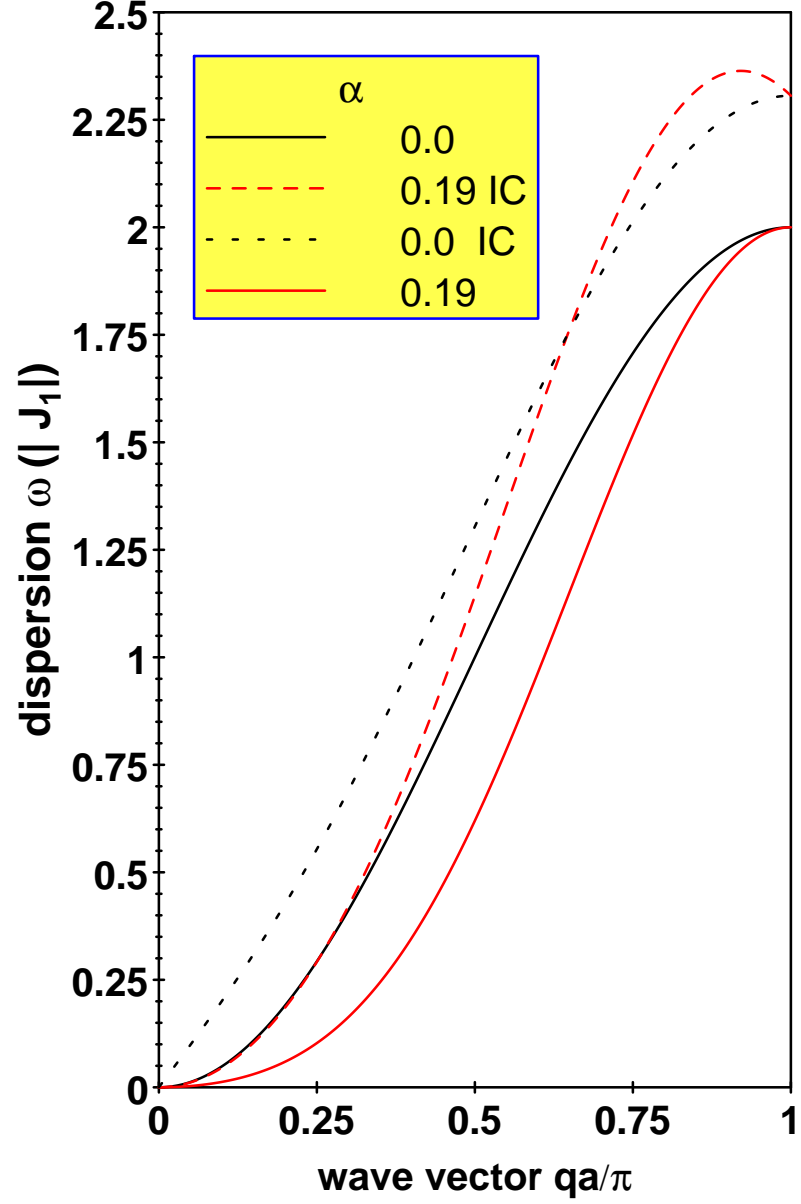


Figure S2: (Color) The influence of the frustration  $\alpha$  on the dispersion of magnetic excitation for a direction affected by the interchain coupling (IC) e.g. (H,0,0) (see Figs. 2 and 3 of the main text). Black curves: no inchain frustration, red curves: inchain frustration included. Broken curves:  $J_{ic}$  included, but we adopt  $J'_{ic}=0$  for the sake of simplicity.

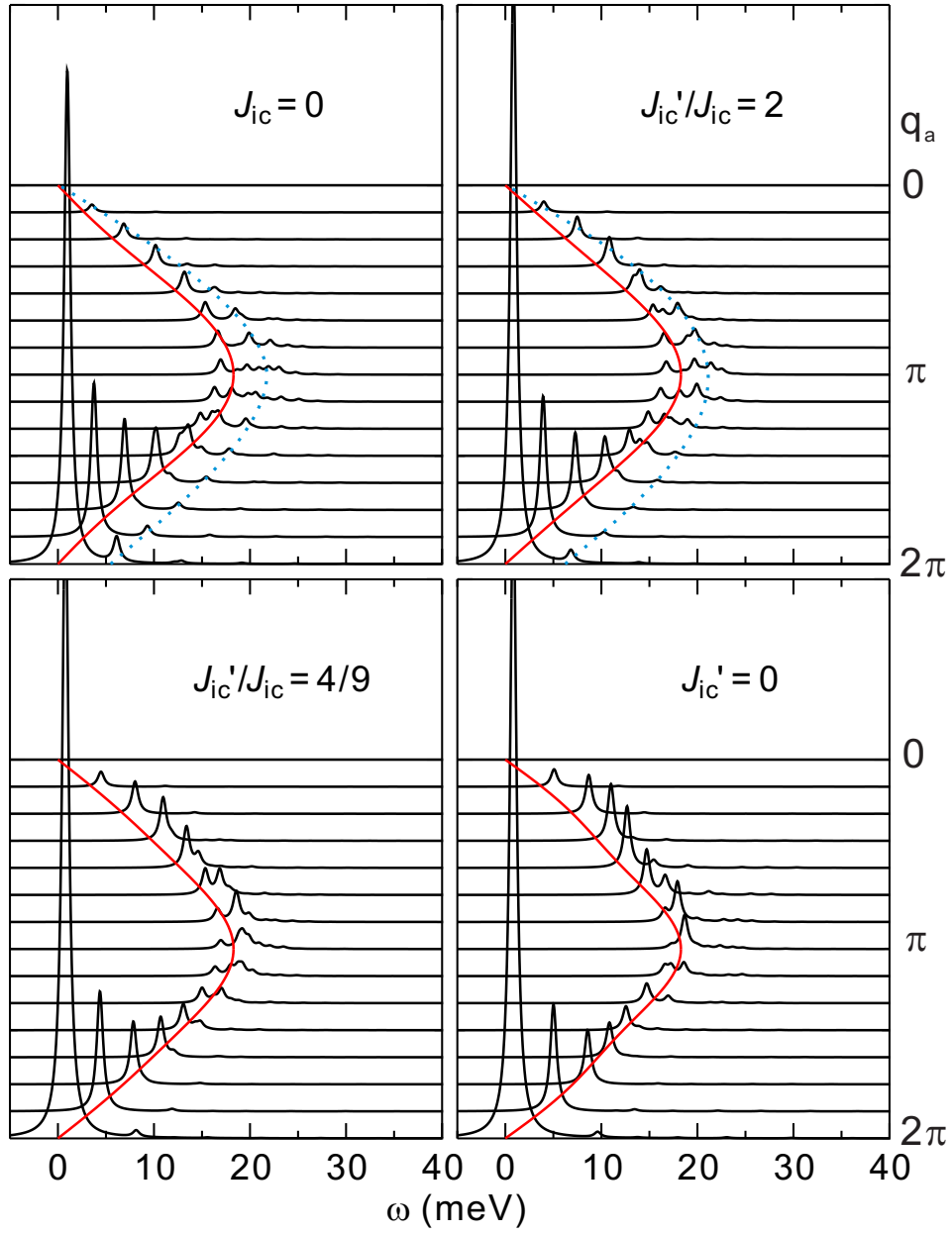


Figure S3: The dynamical structure factor from exact diagonalizations of two coupled chains with 14 sites for each chain at various energies  $\omega$  and momenta  $q$ . Red line: projected maximum position of  $S(\omega, q)$  very close to the LSWT result. Blue dashed line: intensity from the weak minority peaks and the inchain parameters proposed in Ref. 1.



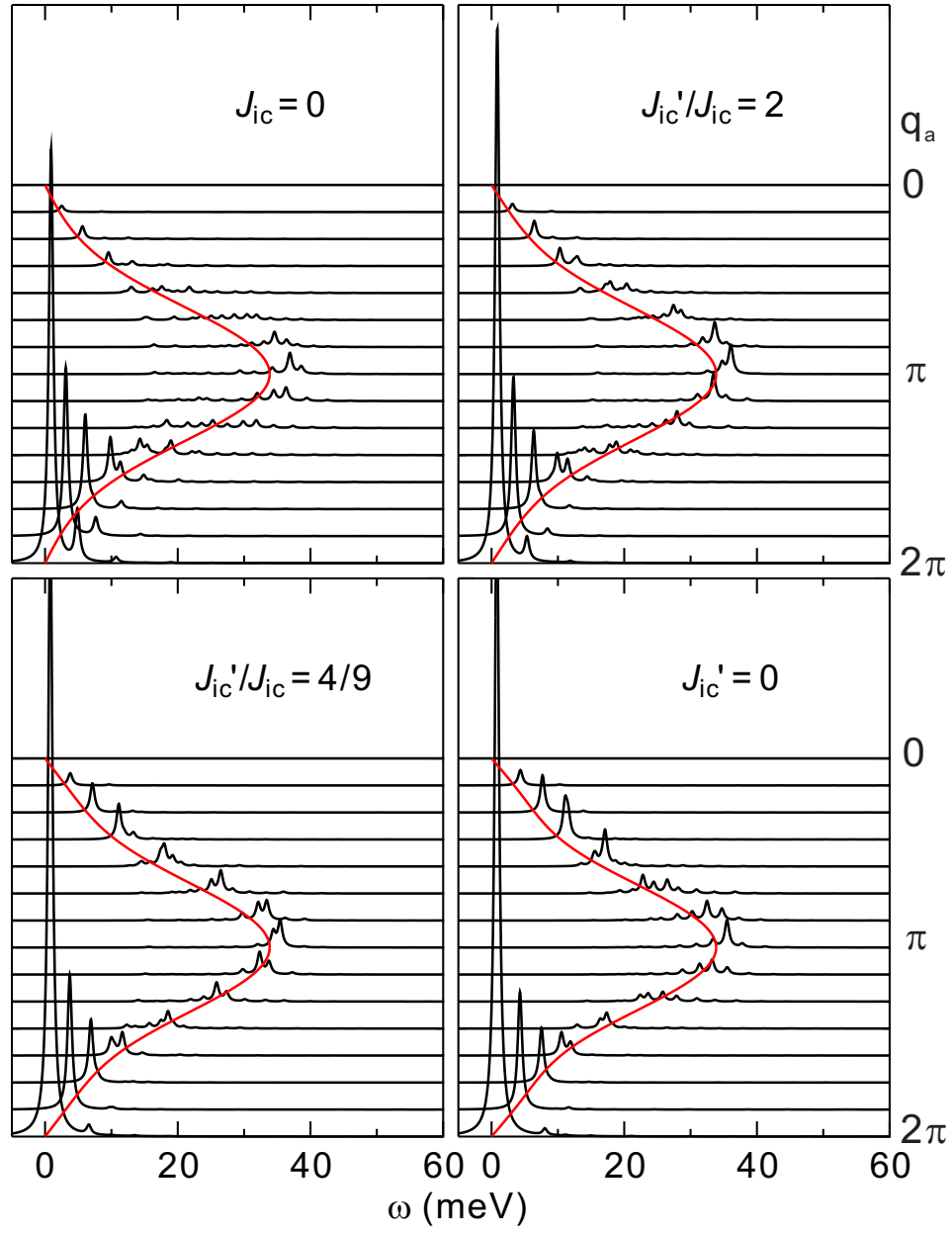


Figure S4: (Color) The same as in Fig. S3 for the new parameter set given in the main text.

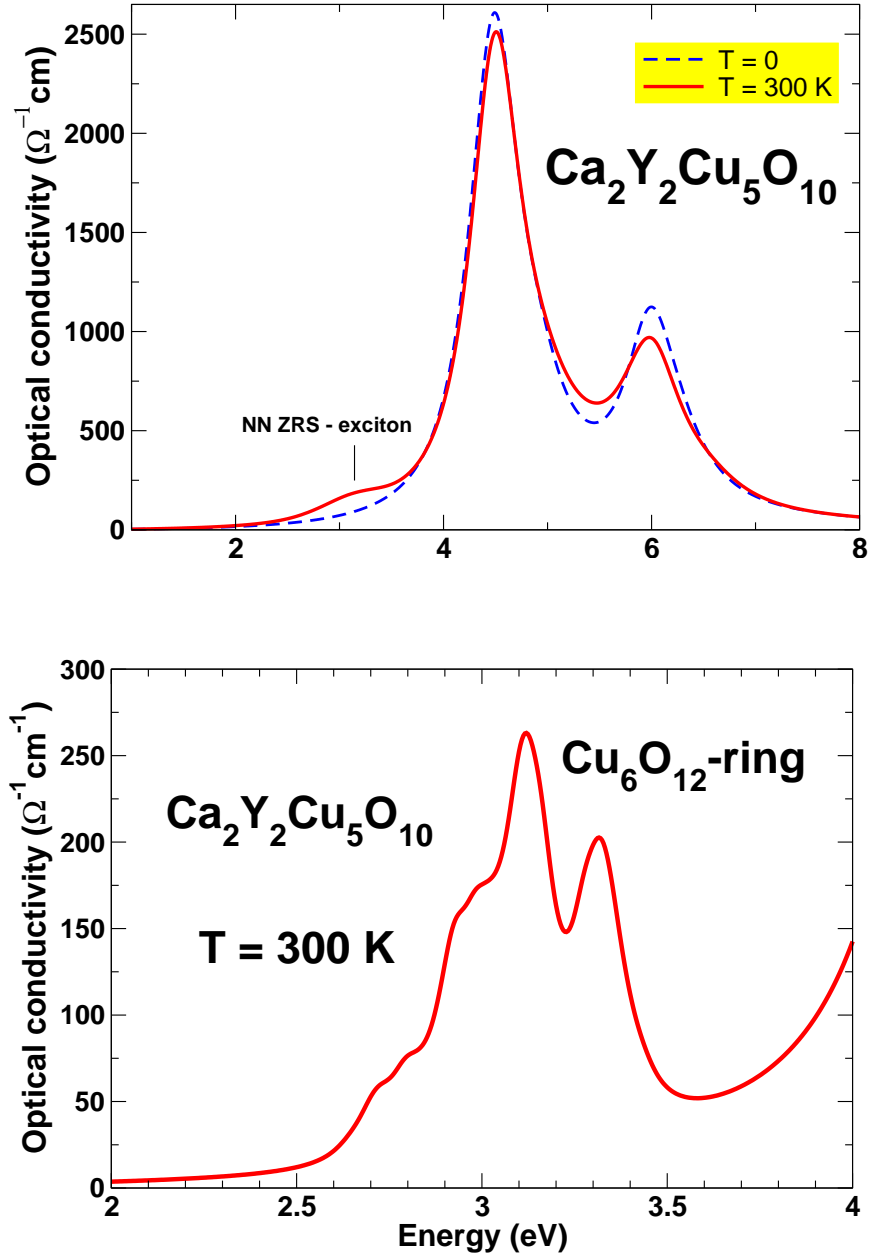


Figure S5: (Color) The optical conductivity  $\sigma(\omega)$  for a  $\text{Cu}_6\text{O}_{12}$  cluster with periodic boundary conditions within the 5-band extended Hubbard  $\text{Cu } 3d \text{ O}2p$  model and parameters given in the main text. Upper: Broad energy region and spectrum broadened by  $\Gamma = 0.3$  eV. Notice the NN Zhang-Rice exciton visible in the spectrum at 300 K and its lacking at  $T = 0$  (compare Fig. 5. in the main text). Lower: The same as in the upper for the region of Zhang-Rice singlet transitions. The spectrum has been broadened by  $\Gamma = 0.05$  eV, only, to make all transitions visible. Notice the main Zhang-Rice singlet exciton near 3 eV.

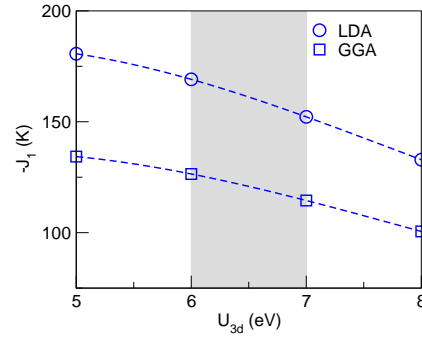


Figure S6: (Color online) Calculated FM NN exchange  $J_1$  as function of the Coulomb repulsion  $U_{3d}$ .

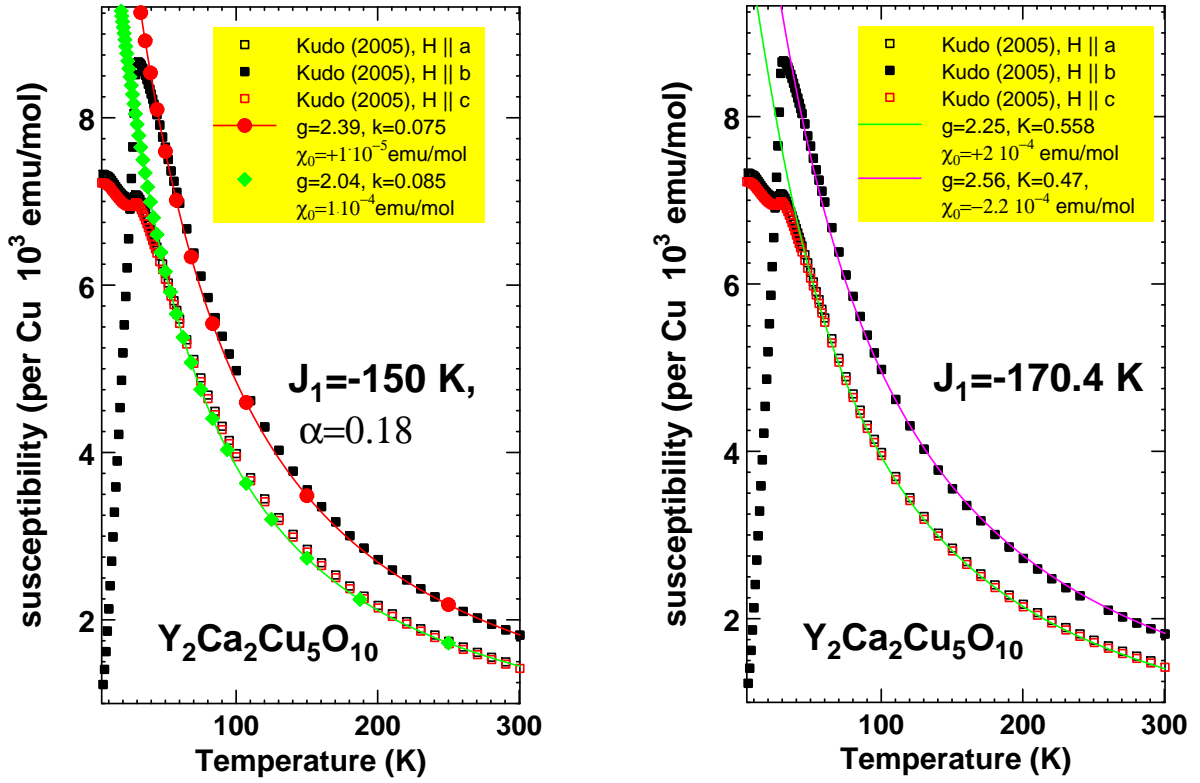


Figure S7: (Color) Left: spin susceptibility  $\chi(T)$  fitted within the 1D  $J_1$ - $J_2$  model supplemented with isotropic AFM IC in 2D treated within the RPA. The latter is measured by the parameter  $k = 2(J'_{ic} + J_{ic}) / |J_1|$ . Right: The same as left for an anisotropic easy-axis inchain coupling  $J_1$ .